Published in final edited form as:
J Neuropathol Exp Neurol. 2012 September ; 71(9): 806–813. doi:10.1097/NEN.0b013e31826775a1.

Gadolinium and 5-Aminolevulinic Acid-induced Protoporphyrin IX Levels in Human Gliomas: An Ex Vivo Quantitative Study to Correlate Protoporphyrin IX Levels and Blood-Brain Barrier Breakdown

Pablo A. Valdés, PhD[*,1,2,6], **Ziev B. Moses, MD**[*,1], **Anthony Kim, PhD**[3], **Clifford J. Belden, MD**[4], **Brian C. Wilson, PhD**[3], **Keith D. Paulsen, PhD**[2,3,5], **David W. Roberts, MD**[5,6], and **Brent T. Harris, MD, PhD**[7]

[1]Dartmouth Medical School, Dartmouth College, Hanover New Hampshire (PAV, ZBM, KDP, DWR, BTH)

[2]Thayer School of Engineering, Dartmouth College, Hanover New Hampshire (PAV, KDP, DWR)

[3]Ontario Cancer Institute, University Health Network of Toronto, Toronto, Ontario, Canada (AK, BCW)

[4]Department of Radiology, Dartmouth Hitchcock Medical Center, Lebanon, New Hampshire (KDP, DWR)

[5]Norris Cotton Cancer Center, Dartmouth Hitchcock Medical Center, , Lebanon, New Hampshire (KDP, DWR)

[6]Section of Neurosurgery (DWR), Department of Radiology (CJB), and Department of Neurology (BTH), Dartmouth-Hitchcock Medical Center, Lebanon, New Hampshire

[7]Departments of Neurology and Pathology, Georgetown University Medical Center, Washington, DC (BTH)

Abstract

In recent years, 5-aminolevulinic acid (ALA)-induced protoporphyrin IX (PpIX) fluorescence guidance has been used as a surgical adjunct to improve the extent of resection of gliomas. Exogenous administration of ALA prior to surgery leads to the accumulation of red fluorescent PpIX in tumor tissue that the surgeon can visualize and thereby discriminate between normal and tumor tissue. Selective accumulation of PpIX has been linked to numerous factors, of which blood-brain barrier (BBB) breakdown has been suggested to be a key factor. To test the hypothesis that PpIX concentration (C_{PpIX}) positively correlates with gadolinium (Gd) concentrations (C_{Gd}), we performed ex vivo measurements of PpIX and of Gd using Inductively-Coupled Plasma Mass Spectrometry (ICP-MS) the latter as a quantitative biomarker of BBB breakdown; this was corroborated with immunohistochemistry of microvascular density in surgical biopsies of patients undergoing fluorescence guided surgery for glioma .We found positive correlations between C_{PpIX} and C_{Gd} ($r = 0.58$, $p < 0.0001$), and between C_{PpIX} and microvascular density ($r = 0.55$, $p <$

Correspondence and reprint requests to: Brent T. Harris, MD, PhD, Director of Neuropathology Department of Neurology, Bldg. D, Rm. 207, 4000 Reservoir Rd, NW, Georgetown University Medical Center, Washington, DC 20057. bth@georgetown.edu.
*These authors contributed equally to this work.

0.0001), suggesting a significant, yet limited association between BBB breakdown and ALA-induced PpIX fluorescence. To our knowledge, this is the first time that Gd measurements by ICP-MS have been used in human gliomas.

Keywords

5-aminolevulinic acid; Contrast enhancement on magnetic resonance imaging; Fluorescence guided surgery; Gadolinium; Mass spectrometry; Microvascular density; Protoporphyrin IX

INTRODUCTION

The extent of resection (EOR) has been shown to correlate with survival and quality of life in patients treated for gliomas. Early post-operative, gadolinium (Gd)-enhanced, T1-weighted magnetic resonance (MR) imaging is used to determine EOR in patients with high-grade gliomas. This method has been shown to be more accurate than intraoperative surgical estimation of EOR, and several studies have shown that removal of contrast-enhancing tissue is a useful prognostic factor (1-4).

Another technique that shows promise for improving assessment of EOR is 5-aminolevulinic acid (ALA)-induced protoporphyrin IX (PpIX) fluorescence-guided resection (FGR) (5-12). With this technique, the patient receives an oral dose of ALA, a precursor in the heme biosynthetic pathway, approximately 3 hours prior to surgery. Exogenous administration of ALA leads to selective accumulation of the fluorescent biomarker PpIX in tumor tissues. Adequate fluorescence imaging adaptations to the surgical microscope allow the surgeon to visualize the red fluorescence from PpIX that is due to selective concentration in tumor tissue; this permits the surgeon to discriminate between normal and tumor tissue. ALA-induced PpIX FGR provides real-time feedback on the presence of tumor in the operating field independent of brain shift and deformation that degrade the accuracy of pre-operative MR image-guidance (6, 13-16).

In view of the utility of T1-weighted contrast-enhanced images for image-guidance, understanding the relationship between PpIX fluorescence and contrast enhancement is important for optimizing the combined use of MRI and FGR for surgical guidance. In a study of 52 patients undergoing ALA-induced PpIX FGR, Stummer et al observed that 16 of 17 patients who had complete removal of strongly visible fluorescent tissue had no residual enhancement on post-operative MR images (8). In addition, our group has shown a strong correlation between contrast enhancement on pre-operative MR imaging and PpIX fluorescence from spatially co-registered tissue specimens (7). These findings suggest a strong, qualitative relationship between fluorescence and contrast enhancement on MR imaging.

To date, these FGR studies with ALA-induced PpIX have reported on the qualitative appearance of PpIX fluorescence in tissues. However, it is well known in biomedical optics that the intrinsic light absorption and scattering properties of tissue can affect the observed fluorescence, making visual assessment of PpIX fluorescence prone to subjectivity (16-19). We have recently developed a highly sensitive and quantitative method for determining PpIX concentrations in vivo that is based on point fluorescence and diffuse reflectance spectroscopy in which the latter is used to correct for the light attenuation in tissue. We showed that tumor with 2 to 3 orders of magnitude more PpIX than surrounding normal brain may not display visible fluorescence using current surgical microscope fluorescence instruments, and that, as expected, visible fluorescence and accumulated levels of PpIX do not follow a linear trend (16).

Gd complexes are used as contrast agents for MR imaging and have been used in models of many conditions including stroke, meningitis and brain tumors in the evaluation of blood-brain barrier (BBB) breakdown (20-25). Selective accumulation of PpIX after ALA administration is likely due to multiple factors (e.g. tumor cell metabolic rate, availability of ferrochelatase enzyme to convert PpIX to heme) in addition to ALA penetration into tumor due to BBB breakdown. Hence, in an effort to quantify the relationship between the BBB breakdown and PpIX levels, we performed ex vivo measurements of PpIX and Gd concentrations in surgical biopsies of patients undergoing FGR for glioma to test the hypothesis that C_{PpIX} correlates with Gd concentrations (C_{Gd}) .Measurements of C_{Gd} by Inductively-Coupled Plasma Mass Spectrometry (ICP-MS) were used as a quantitative biomarker of BBB breakdown and were corroborated with immunohistochemical assessment of microvascular density (MVD) and tumor cell density/grade. To the best of our knowledge, no study has performed ex vivo assessment of Gd concentrations in human brain tumors. We used concentrations of Gd measured using ICP-MS as a metric of BBB breakdown to quantify the relationship between BBB breakdown and increased absolute levels of PpIX (26-37).

MATERIALS AND METHODS

Patient Selection

Individuals aged 18 and older with a preoperative diagnosis of presumed low- or high-grade glioma, and who had tumor judged to be suitable for open cranial resection based on preoperative imaging (as assessed by the study surgeon) were eligible for trial participation. Exclusion criteria included the following: pregnancy or breast feeding, history of cutaneous photosensitivity, hypersensitivity to porphyrins, photodermatosis, exfoliative dermatitis, history of liver disease within the last 12 months, ALT, AST, ALP, or bilirubin levels greater than 2.5 times the normal limit at any time during the previous 2 months, plasma creatinine in excess of 180 mmol/L, inability to comply with the photosensitivity precautions associated with the study, serious associated psychiatric illness, and inability to give informed consent. The FGR protocol was approved by the Dartmouth-Hitchcock Medical Center Committee for the Protection of Human Subjects.

Surgical Procedure

Pre-operative T1-weighted, Gd-enhanced, and/or T2-weighted MR-axial images were obtained for each patient. Approximately 3 hours before induction of anesthesia, patients were administered a 20 mg/kg body weight oral dose of ALA (DUSA Pharmaceuticals, Tarrytown, NY) dissolved in 100 mL water. Surgery was performed using a microscope equipped for fluorescence-guided resection (Zeiss OPMI Pentero®) and neuronavigation was provided via a Medtronic StealthStation® Treon® (Medtronic, Louisville, CO).

Conventional neurosurgical technique with white light illumination and neuronavigational assistance was used. At various times throughout the procedure, the surgeon switched from white light to blue light in order to visualize fluorescence prior to tissue resection (Video, Supplemental Digital Content 1, http://links.lww.com/NEN/A363). Biopsy sites were assigned a fluorescence intensity score by the study surgeon of 0 = no fluorescence, 1 = low fluorescence, 2 = moderate fluorescence, or 3 = high fluorescence. The small (2 – 10 mm in greatest dimension) excised tissue biopsies were then immediately separated into 3 equal parts. The first part was placed into formalin; the second part was placed in a cryogenic vial and snap frozen in liquid N_2; the third part was placed in Optimal Cutting Temperature compound and also stored in liquid N_2. At no point was tissue resected based solely on fluorescence levels (i.e. pre-operatively planned MR imaging features and/or anatomical landmarks and gross appearance of tissue dictated resectable regions). The resection was

considered complete when the surgeon judged that no more tumor tissue was present that could safely be resected using both the microscope and neuronavigation.

Histopathology

Formalin-fixed paraffin-embedded biopsy tissue was processed for hematoxylin and eosin (H&E) staining. A single neuropathologist (B.T.H.) analyzed the H&E-stained specimens blinded to the pathological diagnosis derived from the main surgical specimen. Three histological parameters were measured for each specimen: histopathological score, tumor burden, and necrotic burden (7, 12). The histopathological score was determined on each section using current World Health Organization grading criteria with modification, as follows: (0) = normal and fully necrotic tissue with no viable tumor cells observed; (I) = low number of infiltrating tumor cells (reserved for specific types of glial or glioneuronal neoplasms such as pilocytic astrocytomas, dysembryoplastic neuroepithelial tumors, and gangliogliomas); (II) = higher numbers of infiltrating, pleomorphic cells and no observable necrosis, mitotic figures, or endothelial cell proliferation; (III) = highly pleomorphic tumor cells with mitotic figures, increased neoplastic cell density and no observable necrosis or endothelial cell proliferation, (IV) = highly pleomorphic tumor cells with mitotic figures, increased neoplastic cell density, and either observable necrosis and/or endothelial cell proliferation). Tumor burden (0-III) was determined by comparing the area of tumor tissue with non-tumor tissue on H&E-stained sections with the following criteria used for scoring: 0, normal or fully necrotic tissue section with no observable or viable tumor cells; I, >0% and ≤33% viable tumor; II, >33% and ≤67% viable tumor; and III, >67% viable tumor. Necrotic burden was similarly determined with the following criteria used for scoring: 0, no observable necrosis; I, >0% and ≤33% necrosis; II, >33% and ≤67% necrosis; and III, >67% necrosis. A total of 9 patients with 69 biopsy sites were analyzed with diagnoses from the main surgical specimens as follows: 2 dysembryoplastic neuroepithelial tumors (Grade I); 1 diffuse astrocytoma (Grade II); 4 glioblastoma (Grade IV); and 2 recurrent glioblastoma (Grade IV).

Immunohistochemistry

For all specimens, 4-μm-tissue sections adjacent to tissue processed for H&E were immunostained for CD-31, a pan-endothelial cell marker. In brief, sections were deparaffinized in xylene, rehydrated through graded ethanol solutions to distilled water, and then washed in phosphate-buffered saline. Antigens were retrieved at 125°C using Citra Plus Antigen Retrieval solution (Biogenex, San Ramon, CA) in a pressure cooker for 15 minutes. Endogenous peroxidase activity was quenched using a 3% H_2O_2 block (Biogenex) for 10 minutes. Endogenous avidin binding sites, biotin, and biotin receptors were blocked using avidin and biotin blocking solutions (Biogenex), each for 15 minutes. Non-specific binding sites were blocked using Power Block solution (Biogenex). Tissue sections were incubated overnight at 4°C with mouse monoclonal antibody against CD-31 (clone JC70A, 1:40, Dako, Carpinteria, CA). The following day, tissue sections were incubated with biotinylated goat anti-immunoglobulins (Biogenex) for 30 minutes, followed by horseradish peroxidase-conjugated streptavidin (Biogenex) for 30 minutes. Slides were then developed for 12 minutes with liquid 3-3′-diaminobenzidine substrate (Biogenex), counterstained with hematoxylin, mounted and coverslipped. Appropriate negative controls were routinely obtained by substitution of the primary antibody with phosphate-buffered saline.

Digital images from vascular ‘hot spots’ in 3 representative areas of each immunostained biopsy specimen were captured at 400x magnification using a bright field microscope (Olympus BX2) connected to a digital camera by an investigator (Z.M.), who was blinded to the diagnosis. The images were examined using software (ImagePro Plus 6.2, Bethesda, MD) setup to apply chromogen masks for high-chromogenic staining (brown threshold) and

counterstaining (blue threshold). A vessel density percentage was digitally obtained for each image by calculating the area percentage of stained blood vessels occupying the area of counterstained tissue. The 3 values for each biopsy were averaged to obtain MVD. Figure 1 demonstrates 2 illustrative examples of areas representing high MVD and low MVD, with their corresponding MR and intraoperative blue light images.

Ex Vivo PpIX Fluorometry

Tissue samples (n = 69) were stored in a cryogenic vial at -80°C prior to PpIX quantification. The tissue was combined with 1 ml of Solvable (Dupont-Biotechnology Systems, Boston, MA) and placed in an undulating water bath at 50°C for 1 hour, following a modified protocol from Lilge et al (33). The material was then homogenized with a Tissue Tearor tool in the original vial. The homogenate (500 μL) was then combined with 1.125 ml of distilled water and 0.375 ml of Solvable. After incubation in a 50°C water bath for 1 hour, a spectrophotometer was used to ensure an optical density of less than 0.1. The solution was transferred to a quartz cuvette and was analyzed with a spectrofluorometer using an excitation wavelength of 401 nm. A look-up curve for quantification of PpIX was generated using known serial dilutions of PpIX.

Total tissue fluorescence was modeled as a linear combination of contributions from PpIX, its photoproducts (23), and tissue autofluorescence (24). Several fluorescent components known to exist in brain, including nicotinamide adenine dinucleotide, flavin adenine dinucleotide and lipofuscin, were combined in a linear model to reflect tissue autofluorescence. A pseudoinverse calculation was used to extract the contribution from each product and determine the C_{PpIX} in each tissue (12).

Gd ICP-MS Assay and Contrast-Enhanced MR imaging

Tissue samples (n = 69) stored at -80°C were used for ICP-MS quantification of Gd. Samples ranging from 1 to 40 mg in weight were dissolved in 0.5 ml of nitric acid (60 M) and 100 ml of 30% H_2O_2 by heating in a water bath for 30 minutes and allowed to cool down. The resulting solution was then mixed with 4.5 ml of deionized water. The samples were then analyzed for Gd concentration (C_{Gd}) by ICP-MS (7500cx, Agilent, Santa Clara, CA) at the Dartmouth Trace Element Analysis Core.

Post-injection Gd enhancement on T1-weighted images was assessed for each specimen. MR image coordinates for each specimen were determined using the StealthStation navigation coordinates, and each specimen was assessed for enhancement or no enhancement on MR imaging.

Statistical Analysis

All data were assessed for normality of distribution with Kolmogorov-Smirnov analyses. Correlations between parametric and non-parametric variables were analyzed using Pearson's and Spearman's-rank correlation tests, respectively. Wilcoxon-rank sum (Mann-Whitney) tests were used to determine significant differences between groups. To account for multiple samples from each patient, a clustered data analysis of variance was performed. Differences in visible fluorescence and C_{PpIX}, C_{Gd}, or MVD were summarized with medians and interquartile ranges. Results were considered statistically significant for $p < 0.05$. Data were processed with MATLAB software (Version 2010a, The Mathworks, Inc., Natick, MA). Statistical analyses were carried out using STATA 11.0 (Stata Corporation, College Station, TX).

RESULTS

Relationship Between Intraoperative Visible Fluorescence Levels, C_{PpIX}, C_{Gd} and MVD

Wilcoxon rank sum tests with subsequent validation using a clustered data analysis of variance to account for multiple samples from each patient were used to determine whether there were significant differences between fluorescing and non-fluorescing tissue and levels of C_{PpIX}, C_{Gd}, and MVD. We observed highly statistically significant differences ($p < 0.0001$) with increased C_{Gd}, C_{PpIX} and MVD in visibly compared to non-visibly fluorescent tissues (Fig. 2). Further, we have previously shown a significant correlation between visual fluorescence and C_{PpIX}. In the present study, using a non-parametric Spearman's rank analysis, we tested whether a significant correlation exists between levels of visible fluorescence (0–3) and the 3 quantitative variables – C_{PpIX} C_{Gd} and MVD. We found a strong correlation between increasing levels of intraoperative visible fluorescence and C_{PpIX} ($r = 0.64$, $p < 0.0001$), C_{Gd} ($r = 0.56$, $p < 0.0001$) and MVD ($r = 0.61$, $p < 0.0001$).

Relationship Between C_{PpIX}, C_{Gd} and MVD

We assessed the levels of MVD as an immunohistochemical marker of neovascularization and concomitant BBB breakdown (38-41). The range for C_{PpIX} in the biopsy samples was 0.01 μg/ml to 30.94 μg/ml (mean = 1.62 μg/ml). The range for C_{Gd} in the samples was 0.03 μg/g to 19.83 μg/g (mean = 2.97 μg/g). The range for MVD in samples was 0.07 % to 29.10 % (mean = 5.52%) (Table). Kruskal-Wallis analysis with a Dunn's post-test showed high statistical significance for increasing histopathological scores and C_{Gd} ($p = 0.0010$), and between increasing histopathological scores and MVD ($p < 0.0001$) (Fig. 3). We also found a significant correlation between C_{Gd} and histopathological score ($r = 0.59$, $p < 0.0001$), as well as between MVD and histopathological score ($r = 0.71$, $p < 0.0001$). These results indicate that C_{Gd} and MVD increase with increasing tissue histopathological grade.

Using a Pearson's correlation analysis to assess the role of BBB breakdown and accumulation of PpIX in tissue at a quantitative level, we assessed the correlation (on a log-log scale) between C_{Gd} and CPpIX and between MVD and C_{PpIX}. We found similar significant correlations between C_{Gd} and CPpIX ($r = 0.58$, $p < 0.0001$) and between MVD and C_{PpIX} ($r = 0.55$, $p < 0.0001$), suggesting increasing levels of PpIX with increasing levels of Gd and microvasculature density in tissue. We also found a strong correlation (on a log-log scale) between C_{Gd} and MVD ($r = 0.71$ $p < 0.0001$), reflecting the higher levels of BBB breakdown with increasing levels of brain tumor microvasculature. The strong correlation between C_{Gd} and MVD suggests that C_{Gd} can be used as a valid surrogate marker of BBB breakdown (Fig. 4).

Relationship Between C_{Gd} and Gd Enhancement on T1-weighted MR Imaging

We assessed the relationship between concentrations of Gd and the surgeon's intraoperative assessment of Gd enhancement on T1-weighted MR images for each specimen. We found a significant difference with increased levels of C_{PpIX} ($p = 0.0013$), C_{Gd} ($p < 0.0001$) and MVD ($p < 0.0001$) in enhancing compared to non-enhancing tissue using a Wilcoxon rank sum test, with subsequent verification of these results with clustered data analysis. In this analysis, despite the fact that there was no correction for intraoperative brain shift and deformation, we still observed a highly statistically significant difference in levels of PpIX, Gd, and MVD in MR-enhancing tissue (Fig. 5).

DISCUSSION

We performed a quantitative assessment of ex vivo measurements of Gd and protoporphyrin IX to determine the relationship between BBB breakdown and PpIX accumulation in 9

patients undergoing FGR for gliomas. Previous studies were limited by intraoperative brain shift and deformation, which hinders the one-to-one association and accuracy in relating intraoperative PpIX fluorescence and contrast enhancement on pre- or post-MR imaging (7, 8, 13-15, 42, 43).

Here we show that C_{Gd}, used as a surrogate biomarker of BBB breakdown, accumulates in significantly higher levels in visibly fluorescent compared to non-visibly fluorescent tissue, and in tissue with higher grade histopathological features. These results support the idea that BBB breakdown plays a significant role in intraoperative levels of accumulated PpIX fluorescence, although it is likely not the only or the major factor. In addition, the significant correlation between C_{PpIX} and C_{Gd} ($r = 0.58$, $p < 0.0001$) suggests that this relationship holds even beyond the ability for the human eye to detect intraoperative visible fluorescence. More importantly, the results show a quantitative relationship between levels of accumulated PpIX in tissue and Gd that are not confounded by the influence of intraoperative brain shift and deformation. To corroborate these results, we analyzed samples that did not show visible fluorescence and found a similarly strong correlation between low C_{PpIX} and low C_{Gd} ($n = 50$, $r = 0.40$, $p = 0.0041$) (data not shown). Further, the significant, yet modest correlation ($r = 0.58$) also highlights the fact that BBB breakdown is not the sole cause of PpIX accumulation but that additional factors likely play a key role in this complex phenomenon.

To validate the use of C_{Gd} as a surrogate marker of BBB breakdown, we performed CD31 immunohistochemical staining and assessed tissue MVD (38-41). As expected, C_{Gd} showed a strong correlation with MVD ($r = 0.71$ $p < 0.0001$). In addition, the similar correlations between C_{PpIX} and C_{Gd} ($r = 0.58$, $p < 0.0001$) and between C_{PpIX} and MVD ($r = 0.55$, $p < 0.0001$) further suggest the validity of using C_{Gd} as a surrogate biomarker of BBB breakdown. The highly statistically significant difference with increasing levels of Gd and MVD observed in contrast enhancing vs. non-contrast enhancing tissue on MR imaging further substantiate these conclusions.

There was a stronger correlation between MVD and Gd concentrations ($r = 0.71$) in tissue compared to the correlation between PpIX levels and our surrogate markers of BBB breakdown, MVD and C_{Gd} ($r = 0.55$ and 0.58, respectively). We hypothesized that Gd accumulation depends mostly on BBB breakdown, and thus a stronger correlation for MVD and Gd concentrations was expected. We have previously shown that PpIX accumulation displays a strong correlation on factors intrinsic to tumor growth (e.g. cellular proliferation) in addition to increased supply of ALA from BBB breakdown. Previously, Ennis et al demonstrated the limited, diffusion dependent availability of ALA to normal brain tissues (44). Ishihara et al found a significant correlation, comparable to our correlation between absolute levels of PpIX ex vivo and MVD, between spectroscopic measurements of PpIX fluorescence and microvasculature density using CD-31 IHC (45). This indicates the importance of microvasculature status in high PpIX levels found in tumors.

Here we observed 2 seemingly distinct, but complementary trends in PpIX accumulation in tumors: an exponential growth trend starting at high C_{Gd} (~3μg/g) and peaking at C_{PpIX} ~10 μg/ml, and an exponential growth trend starting at lower MVD (~0.1%) and saturating at C_{PpIX} ~10 μg/ml. The former trend might suggest that PpIX accumulates at smaller concentrations, in part due to decreased ALA delivery to tissues, i.e. tissue with a lower level of BBB breakdown (as measured by low C_{Gd}), but reaches a peak intracellular level of PpIX at ~ 10 μg/ml, irrespective of ALA availability. Meanwhile, the latter trend at low MVD further points towards a complementary saturation effect, namely that intracellular PpIX accumulation reaches a saturation concentration at ~10 μg/ml.

We previously showed that because PpIX is the main fluorophore in intracranial tissues, visibly fluorescing tissue accumulates a high C_{PpIX} (12, 16). However, tissue optical absorption and scattering attenuate the fluorescence intensity and distort the fluorescence emission spectra; therefore, the actual PpIX concentration and qualitative visible fluorescence do not follow a strictly linear relationship (16-18, 46). Quantitative measurements of C_{PpIX} provide an objective measure of the fluorescent biomarker in tissue, and thus a more accurate assessment of the presence of tumor. Here we compared both the subjective assessments of PpIX fluorescence and quantitative measurements of PpIX, together with quantitative metrics of BBB breakdown, to obtain a more comprehensive and accurate understanding of the relationship between PpIX fluorescence and the role of the BBB.

Stummer et al studied cell density, MIB-1 labeling index and capillary density in 141 biopsies from patients operated for malignant glioma and found a positive correlation between the qualitative intraoperative fluorescence and MIB-1 labeling index and vascular density (11). Although we did not quantify cellular proliferation here, we previously found a correlation between labeling index and intraoperative fluorescence (7, 16). The correlation of C_{Gd} and C_{PpIX} with intraoperative fluorescence most likely reflects alterations in vessel structures that lead to leakiness and Gd or PPIX accumulation, respectively. Stummer et al also found a significant yet limited relationship between MVD and PpIX visual fluorescence intensity scores and concluded that BBB breakdown is one of several factors involved in fluorescence accumulation (11). Currently there is no gold standard by which to measure BBB breakdown with ex vivo tissue slices in humans. Our results are encouraging in that we measured a surrogate of BBB breakdown (i.e. C_{Gd}) rather than intact microvasculature as reflected in the correlation between MVD and Gd concentration (Fig. 4C). Overall, our results are consistent with the report of Stummer et al and suggest that use of ex vivo measurements of Gd in tissue can be used as a surrogate biomarker of BBB breakdown.

We also observed a correlation between increasing histopathologic score and Gd concentrations (Fig. 3) that most likely reflects the enhanced neovascularization and accompanying BBB breakdown in regions of increased malignancy. Further, pre-operative post-contrast injection T1-weighted MR images showed that regions of enhancement were highly associated with increased C_{Gd} vs. non-enhancing regions, despite the confounding effects of intraoperative changes. The strong association between co-registered, preoperative MR image enhancement and tissue levels of Gd further corroborate the ICP-MS measurements.

The limitations of this study include the diversity and numbers of glioma patients studied. Nevertheless, C_{Gd} was consistently associated with both visible levels of fluorescence and PpIX concentrations in tissue. Future work will investigate a larger population of patients and tumor types. Sampling error at the time of sample separation is also a possible limitation of this study. One other limitation includes the use of tissue C_{Gd}s, which are known to decrease rapidly following contrast administration. All samples were obtained within approximately a 4- to 8-hour period from the time of contrast administration to the moment of tissue collection and previous reports suggest that relative changes in concentrations of Gd in tissue should be minimal during this period (30, 37). Previous imaging literature also suggests that Gd is rapidly cleared from blood and because the tissue was obtained a minimum of 4 hours after the administration of Gd, we surmise that Gd present predominantly accumulated in the extravascular space (47, 48). Finally, it is possible that a decrease in the fluorescence signal from PpIX as a result of organic degradation processes could have occurred, but not so for Gd, which is a stable metal. Nevertheless, given the extremely low temperature and light conditions we expect this effect to be minimal. In

addition, the systematic nature of this effect across all specimens, would not affect the overall conclusions regarding strong correlations between PpIX and MVD or C_{Gd}.

In summary, we performed a quantitative assessment of Gd concentrations in tissue as a surrogate marker of BBB breakdown. We found a significant correlation between Gd and PpIX concentrations in patients undergoing FGR for glioma. Further, we validated the use of ex vivo Gd concentrations as a marker of BBB breakdown using a metric of microvasculature density. Our quantitative results further support the significant yet limited impact of BBB breakdown on increased PpIX fluorescence, meanwhile also highlighting the need to understand this complex mechanism and the additional factors that contribute to this phenomenon. This work highlights the relationships of BBB status and quantitative assessments of PpIX in ALA-induced PpIX FGR.

Supplementary Material

Refer to Web version on PubMed Central for supplementary material.

Acknowledgments

This work was supported in part by NIH grant R01NS052274-04 (DWR) awarded by the National Institute of Neurological Disorders and Stroke. The Trace Elements Analysis Core was supported by NIH Grant Number P42 ES007373 from the National Institute of Environmental Health Sciences. Carl Zeiss (Carl Zeiss Surgical GmbH, Oberkochen, Germany) and Medtronic Navigation (Medtronic, Louisville, CO, USA) provided the fluorescence-enabled OPMI Pentero® operating microscope and StealthStation® Treon® navigation system, respectively. DUSA Pharmaceuticals (DUSA Pharmaceuticals, Tarrytown, NY) supplied the ALA.

REFERENCES

1. Albert FK, Forsting M, Sartor K, et al. Early postoperative magnetic resonance imaging after resection of malignant glioma: objective evaluation of residual tumor and its influence on regrowth and prognosis. Neurosurgery. 1994; 34:45–60. discussion -1. [PubMed: 8121569]
2. Lacroix M, Abi-Said D, Fourney DR, et al. A multivariate analysis of 416 patients with glioblastoma multiforme: prognosis, extent of resection, and survival. J Neurosurg. 2001; 95:190–8. [PubMed: 11780887]
3. Sanai N, Berger MS. Glioma extent of resection and its impact on patient outcome. Neurosurgery. 2008; 62:753–64. discussion 264-6. [PubMed: 18496181]
4. Sanai N, Polley MY, McDermott MW, et al. An extent of resection threshold for newly diagnosed glioblastomas. J Neurosurg. 2011; 115:3–8. [PubMed: 21417701]
5. Pichlmeier U, Bink A, Schackert G, et al. Resection and survival in glioblastoma multiforme: an RTOG recursive partitioning analysis of ALA study patients. Neuro Oncol. 2008; 10:1025–34. [PubMed: 18667747]
6. Pogue BW, Gibbs-Strauss S, Valdes PA, et al. Review of Neurosurgical Fluorescence Imaging Methodologies. IEEE J Sel Top Quantum Electron. 2010; 16:493–505. [PubMed: 20671936]
7. Roberts DW, Valdes PA, Harris BT, et al. Coregistered fluorescence-enhanced tumor resection of malignant glioma: relationships between delta-aminolevulinic acid-induced protoporphyrin IX fluorescence, magnetic resonance imaging enhancement, and neuropathological parameters. J Neurosurg. 2011; 114:595–603. [PubMed: 20380535]
8. Stummer W, Novotny A, Stepp H, et al. Fluorescence-guided resection of glioblastoma multiforme by using 5-aminolevulinic acid-induced porphyrins: a prospective study in 52 consecutive patients. J Neurosurg. 2000; 93:1003–13. [PubMed: 11117842]
9. Stummer W, Pichlmeier U, Meinel T, et al. Fluorescence-guided surgery with 5-aminolevulinic acid for resection of malignant glioma: a randomised controlled multicentre phase III trial. Lancet Oncol. 2006; 7:392–401. [PubMed: 16648043]

10. Stummer W, Reulen HJ, Meinel T, et al. Extent of resection and survival in glioblastoma multiforme: identification of and adjustment for bias. Neurosurgery. 2008; 62:564–76. discussion -76. [PubMed: 18425006]
11. Stummer W, Reulen HJ, Novotny A, et al. Fluorescence-guided resections of malignant gliomas--an overview. Acta Neurochir Suppl. 2003; 88:9–12. [PubMed: 14531555]
12. Valdes PA, Kim A, Brantsch M, et al. δ-aminolevulinic acid-induced protoporphyrin IX concentration correlates with histopathological markers of malignancy in human gliomas: the need for quantitative fluorescence-guided resection to identify regions of increasing malignancy. Neuro Oncol. 2011; 13:846–56. [PubMed: 21798847]
13. Roberts DW, Miga MI, Hartov A, et al. Intraoperatively updated neuroimaging using brain modeling and sparse data. Neurosurgery. 1999; 45:1199–206. discussion 206-7. [PubMed: 10549938]
14. Sun H, Lunn KE, Farid H, et al. Stereopsis-guided brain shift compensation. IEEE Trans Med Imaging. 2005; 24:1039–52. [PubMed: 16092335]
15. Valdes PA, Fan X, Ji S, et al. Estimation of brain deformation for volumetric image updating in protoporphyrin IX fluorescence-guided resection. Stereotact Funct Neurosurg. 2010; 88:1–10. [PubMed: 19907205]
16. Valdes PA, Leblond F, Kim A, et al. Quantitative fluorescence in intracranial tumor: implications for ALA-induced PpIX as an intraoperative biomarker. J Neurosurg. 2011; 115:11–7. [PubMed: 21438658]
17. Kim A, Khurana M, Moriyama Y, et al. Quantification of in vivo fluorescence decoupled from the effects of tissue optical properties using fiber-optic spectroscopy measurements. J Biomed Opt. 2010; 15:067006. [PubMed: 21198210]
18. Richards-Kortum R, Sevick-Muraca E. Quantitative optical spectroscopy for tissue diagnosis. Annu Rev Phys Chem. 1996; 47:555–606. [PubMed: 8930102]
19. Weersink R, Patterson MS, Diamond K, et al. Noninvasive measurement of fluorophore concentration in turbid media with a simple fluorescence /reflectance ratio technique. Appl Opt. 2001; 40:6389–95. [PubMed: 18364948]
20. Dijkhuizen RM, Nicolay K. Magnetic resonance imaging in experimental models of brain disorders. J Cereb Blood Flow Metab. 2003; 23:1383–402. [PubMed: 14663334]
21. Ichikawa H, Itoh K. Blood-arachnoid barrier disruption in experimental rat meningitis detected using gadolinium-enhancement ratio imaging. Brain Res. 2011; 1390:142–9. [PubMed: 21435335]
22. Knight RA, Barker PB, Fagan SC, et al. Prediction of impending hemorrhagic transformation in ischemic stroke using magnetic resonance imaging in rats. Stroke. 1998; 29:144–51. [PubMed: 9445344]
23. Runge VM, Price AC, Wehr CJ, et al. Contrast enhanced MRI. Evaluation of a canine model of osmotic blood-brain barrier disruption. Invest Radiol. 1985; 20:830–44. [PubMed: 4077437]
24. Schmiedl UP, Kenney J, Maravilla KR. Dyke Award Paper. Kinetics of pathologic blood-brain-barrier permeability in an astrocytic glioma using contrast-enhanced MR. AJNR Am J Neuroradiol. 1992; 13:5–14. [PubMed: 1595491]
25. Warach S, Latour LL. Evidence of reperfusion injury, exacerbated by thrombolytic therapy, in human focal brain ischemia using a novel imaging marker of early blood-brain barrier disruption. Stroke. 2004; 35:2659–61. [PubMed: 15472105]
26. Deeken JF, Loscher W. The blood-brain barrier and cancer: transporters, treatment, and Trojan horses. Clin Cancer Res. 2007; 13:1663–74. [PubMed: 17363519]
27. Loreti V, Bettmer J. Determination of the MRI contrast agent Gd-DTPA by SEC-ICP-MS. Anal Bioanal Chem. 2004; 379:1050–4. [PubMed: 15235758]
28. Weinmann HJ, Brasch RC, Press WR, et al. Characteristics of gadolinium-DTPA complex: a potential NMR contrast agent. AJR Am J Roentgenol. 1984; 142:619–24. [PubMed: 6607655]
29. Kamaly N, Pugh JA, Kalber TL, et al. Imaging of gadolinium spatial distribution in tumor tissue by laser ablation inductively coupled plasma mass spectrometry. Mol Imaging Biol. 2010; 12:361–6. [PubMed: 19921340]
30. Kindberg GM, Uran S, Friisk G, et al. The fate of Gd and chelate following intravenous injection of gadodiamide in rats. Eur Radiol. 2010; 20:1636–43. [PubMed: 20157815]

31. Miles DR, Mesfin M, Mody TD, et al. Validation and use of three complementary analytical methods (LC-FLS, LC-MS/MS and ICP-MS) to evaluate the pharmacokinetics, biodistribution and stability of motexafin gadolinium in plasma and tissues. Anal Bioanal Chem. 2006; 385:345–56. [PubMed: 16609840]
32. Miles DR, Smith JA, Phan SC, et al. Population pharmacokinetics of motexafin gadolinium in adults with brain metastases or glioblastoma multiforme. J Clin Pharmacol. 2005; 45:299–312. [PubMed: 15703365]
33. Blaum K, Geppert C, Schreiber WG, et al. Trace determination of gadolinium in biomedical samples by diode laser-based multi-step resonance ionization mass spectrometry. Anal Bioanal Chem. 2002; 372:759–65. [PubMed: 12012186]
34. Zhang T, Matsumura A, Yamamoto T, et al. Comparison of gadobenate dimeglumine and gadopentetate dimeglumine: a study of MR imaging and inductively coupled plasma atomic emission spectroscopy in rat brain tumors. AJNR Am J Neuroradiol. 2002; 23:15–8. [PubMed: 11827870]
35. White GW, Gibby WA, Tweedle MF. Comparison of Gd(DTPA-BMA) (Omniscan) versus Gd(HP-DO3A) (ProHance) relative to gadolinium retention in human bone tissue by inductively coupled plasma mass spectroscopy. Invest Radiol. 2006; 41:272–8. [PubMed: 16481910]
36. Frame EM, Uzgiris EE. Gadolinium determination in tissue samples by inductively coupled plasma mass spectrometry and inductively coupled plasma atomic emission spectrometry in evaluation of the action of magnetic resonance imaging contrast agents. Analyst. 1998; 123:675–9. [PubMed: 9684400]
37. De Stasio G, Casalbore P, Pallini R, et al. Gadolinium in human glioblastoma cells for gadolinium neutron capture therapy. Cancer Res. 2001; 61:4272–7. [PubMed: 11358855]
38. Hasan J, Byers R, Jayson GC. Intra-tumoural microvessel density in human solid tumours. Br J Cancer. 2002; 86:1566–77. [PubMed: 12085206]
39. Weidner N, Semple JP, Welch WR, et al. Tumor angiogenesis and metastasis--correlation in invasive breast carcinoma. N Engl J Med. 1991; 324:1–8. [PubMed: 1701519]
40. Vermeulen PB, Gasparini G, Fox SB, et al. Second international consensus on the methodology and criteria of evaluation of angiogenesis quantification in solid human tumours. Eur J Cancer. 2002; 38:1564–79. [PubMed: 12142044]
41. Vermeulen PB, Gasparini G, Fox SB, et al. Quantification of angiogenesis in solid human tumours: an international consensus on the methodology and criteria of evaluation. Eur J Cancer. 1996; 32A:2474–84. [PubMed: 9059336]
42. Lunn KE, Paulsen KD, Roberts DW, et al. Displacement estimation with co-registered ultrasound for image guided neurosurgery: a quantitative in vivo porcine study. IEEE Trans Med Imaging. 2003; 22:1358–68. [PubMed: 14606670]
43. Lunn KE, Paulsen KD, Lynch DR, et al. Assimilating intraoperative data with brain shift modeling using the adjoint equations. Med Image Anal. 2005; 9:281–93. [PubMed: 15854847]
44. Ennis SR, Novotny A, Xiang J, et al. Transport of 5-aminolevulinic acid between blood and brain. Brain Res. 2003; 959:226–34. [PubMed: 12493610]
45. Ishihara R, Katayama Y, Watanabe T, et al. Quantitative spectroscopic analysis of 5-aminolevulinic acid-induced protoporphyrin IX fluorescence intensity in diffusely infiltrating astrocytomas. Neurol Med Chir (Tokyo). 2007; 47:53–7. discussion 7. [PubMed: 17317941]
46. Ramanujam N. Fluorescence spectroscopy of neoplastic and non-neoplastic tissues. Neoplasia. 2000; 2:89–117. [PubMed: 10933071]
47. Runge VM, Schaible TF, Goldstein HA, et al. Gd DTPA. Clinical efficacy. Radiographics. 1988; 8(1):147–59. [PubMed: 3353531]
48. Weinmann HJ, Brasch RC, Press W, et al. Characteristics of gadolinium-DTPA complex: a potential NMR contrast agent. AJR. 1984; 142:619–24. [PubMed: 6607655]

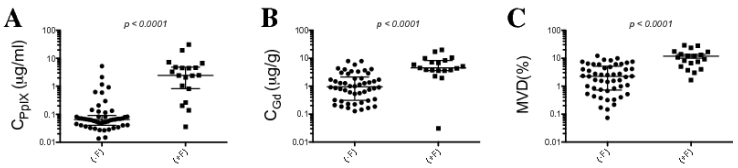

Figure 1.

Examples of co-registered fluorescence-guided resection, pre-operative gadolinium magnetic resonance (MR) imaging, and histopathology in 2 patients with glioblastoma. (**A-F**) Image space coordinates for 2 specimens on pre-operative post-contrast gadolinium injection T1-weighted MR axial images showing a region of contrast enhancing tissue from patient 1 with a high C_{Gd} = 19.830 μg/g (**A**) and contrast non-enhancing tissue from patient 2 with low C_{Gd} = 0.340 μg/g (**D**). Corresponding intra-operative fluorescence images for patient 1 show visible fluorescence and high C_{PpIX} = 2.084 μg/ml (**B**); for patient 2 there is no visible fluorescence and a low C_{PpIX} = 0.081 μg/ml (**E**). Corresponding immunohistochemistry images for patient 1 show high levels of CD31 immunostaining with MVD = 29.10% (**C**); for patient 2 there are low levels of CD-31 staining with a MVD = 0.99%. (**F**). C_{Gd}, gadolinium concentration; C_{PpIX} = protoporphyrin IX concentration; MVD, microvascular density.

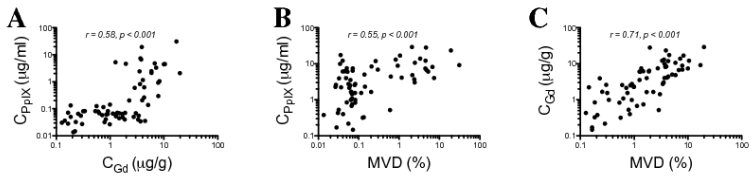

Figure 2.

Protoporphyrin IX (PpIX), gadolinium, MVD and intraoperative visible fluorescence. Median and interquartiles ranges of C_{PpIX} (**A**), C_{Gd} (**B**) and MVD (**C**), in tissues with no visible fluorescence, (-F), or positive visible fluorescence, (+F). Wilcoxon-rank sum (Mann-Whitney) tests were used to determine significant differences between groups, validate these results and account for multiple samples from each patient. A clustered data analysis of variance was additonally performed to validate the results and account for multiple samples from each patient. C_{PpIX} ($p < 0.0001$), C_{Gd} ($p < 0.0001$), and MVD ($p < 0.0001$) were all significantly higher in +F vs. –F tissue. CGd, gadolinium concentration; CPpIX = ;protoporphyrin IX concentration; MVD, microvascular density.

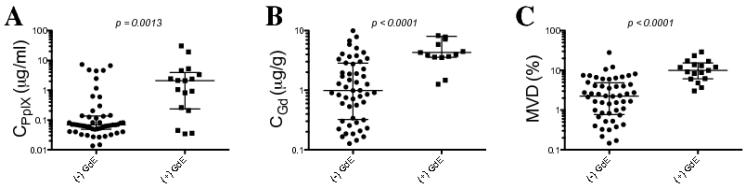

Figure 3.

Increasing gadolinium concentrations and microvasculature density in tissues with higher histopthological scores. Kruskal-Wallis analysis with a Dunn's post-test showed high statistical significance for increasing histopathological scores and C_{Gd} as observed in the scatter plot of C_{Gd} vs. histopathological scores ($p = 0.0010$) as well as increasing histopathological scores and MVD ($p < 0.0001$). C_{Gd}, gadolinium concentration; C_{PpIX} = ;protoporphyrin IX concentration; MVD, microvascular density. Scoring criteria are described in Materials and Methods.

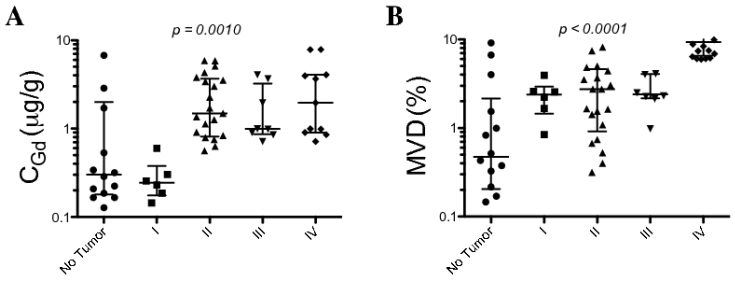

Figure 4.

Blood-brain barrier breakdown and protoporphyrin IX (PpIX) concentrations. Pearson's correlation analysis of scatter plot of log C_{Gd} vs. log C_{PpIX} ($r = 0.58$, $p < 0.0001$) (**A**), scatter plot of log MVD vs. log C_{PpIX} ($r = 0.55$, $p < 0.0001$) (**B**), and scatter plot of log MVD vs. log C_{Gd} ($r = 0.71$, $p < 0.0001$) (**C**). C_{PpIX}, ex vivo PpIX concentration; C_{Gd}, ex vivo gadolinium concentration; MVD, microvasculature density using CD31 immunohistochemical staining.

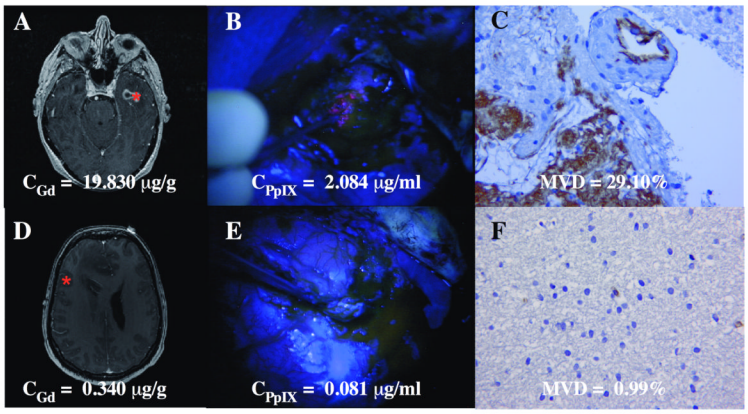

Figure 5.

Contrast-enhanced T1-weighted magnetic resonance (MR) imaging relationships with protoporphyrin IX (PpIX) concentrations, gadolinium concentrations, and microvascular density (MVD). Median and interquartiles ranges of C_{PpIX} (**A**), C_{Gd} (**B**) and MVD (**C**) in non-enhancing, [(−) GdE], or enhancing, [(+) GdE] tissue on post-contrast injection T1-weighted MR imaging. Wilcoxon-rank sum (Mann-Whitney) tests were used to determine significant differences between groups. A clustered data analysis of variance was performed to validate these results and to account for multiple samples for each patient: C_{PpIX} ($p = 0.0013$), C_{Gd} ($p < 0.0001$), and MVD ($p < 0.0001$) were all significantly higher in (+) GdE vs. (−) GdE tissue. C_{Gd}, gadolinium concentration; C_{PpIX} = ;protoporphyrin IX concentration; MVD, microvascular density.

Table

Protoporphyrin IX, Gadolinium, and Microvascular Density Ex Vivo Measurements

	C_{PpIX} (μg/ml)	C_{Gd} (μg/g)	MVD (%)
Minimum	0.013	0.031	0.07
Average	1.616	2.965	5.52
Maximum	30.936	19.830	29.10

C_{PpIX} , protoporyphyrin IX concentration; C_{Gd}, gadolinium concentration; MVD, microvascular density.